Ballistic-electron coherent spin precession in a Rashba two-dimensional electron system

Mark Johnson

U.S. Naval Research Laboratory, Washington, DC 20375, USA

The prodigious career of E. I. Rashba produced numerous creative and novel theoretical discoveries. One contribution that has had significant impact is his theoretical explanation of spin-orbit effects that arise from materials and heterostructures that are characterized by a structural asymmetry. This theory has created entire subfields in condensed matter physics. The focus of this paper is the empirical demonstration of one topic in one of these subfields. Spin-polarized carriers injected into a high-mobility two-dimensional electron system with a Rashba spin-orbit interaction will exhibit conductance oscillations over a length scale of a ballistic mean free path. Two separate experimental demonstrations are discussed.

I. INTRODUCTION

The 1950s decade was a time when pioneering theoretical treatments of spin-orbit interactions in semiconductors were developed [1,2], even though experimental progress was yet to come. In the period 1959–1960, E. I. Rashba derived a theory for the electron energy bands of a semiconductor with a crystal structure lacking inversion symmetry [3–5]. The theory described a spin-orbit interaction that resulted in spin-split subbands. Further theoretical progress was made in the 1960s and 1970s [6]. In the early 1980s, unexplained features in electron spin resonance experiments on two-dimensional modulation-doped semiconductor heterostructures [7] motivated new work. Rashba and Bychkov described a spin-orbit interaction in some two-dimensional electron systems (2DES) with structural inversion asymmetry [8]. These seminal theoretical insights opened new subfields in condensed matter physics. Many decades later, Rashba's impact is evident in currently active topics of research that range from layered two-dimensional materials and novel superconducting materials to quantum computing [9]. This paper discusses two experiments that verified an extraordinary phenomenon that relies on the Rashba spin-orbit interaction.

One theoretical outcome of Rashba's seminal work was the prediction of a novel carrier transport effect by Datta and Das [10]. These authors described a planar field-effect transistor (FET) structure with a source and drain connected by a channel of length L along the x axis. Length L is chosen to be less than a ballistic mean free path of electrons in the channel. When the electrons injected at the source are spin polarized with spin orientation along $\hat{x}$, the spins would precess about the y axis as a consequence of the Rashba spin-orbit interaction (SOI) in the channel. If the drain had a conductance that was sensitive to the spin polarization of the carriers, then the source-drain conductance would have a maximum when the precessional wavelength was equal to L and a minimum when L equaled half a precessional wavelength. In their model, the ballistic carriers in the channel could be represented by a spin-polarized current with spin orientation

that was nearly coherent because all the carriers traveled at the Fermi velocity. Therefore, an experiment would observe that the source drain conductance G_{SD} would show a periodic modulation as a function of channel length L, $G_{SD} \propto L$. There would be no spatial variation of source-drain conductance if the carriers injected at the source were spin polarized with spin orientation along $\hat{y}$. Going a step further, Datta and Das noted that an external gate voltage would modulate the SOI and the rate of precession. Therefore, one could observe the source-drain conductance modulation by keeping L fixed but varying the gate voltage V_G. An experiment would show a periodic conductance modulation as a function gate voltage $G_{SD} \propto V_G$. Two different experimental techniques have verified the unique Datta-Das prediction [11,12]. These experiments involve many cutting edge advances in condensed matter and materials physics: high-mobility two-dimensional electron systems (2DES), ballistic carrier transport, thin ferromagnetic films as spin polarizers for injection and detection of carriers, spin coherence, and the details of interface spin transport.

In a two-dimensional electron system, an intrinsic electric field from inversion asymmetry in the confinement potential of the quantum well will cause a spin-orbit interaction between carrier spin and momentum. Consider an electron in a microstructured, narrow 2DES channel [Fig. 1(a)] with momentum $\vec{k}$ along the $+\hat{x}$ axis, and intrinsic field $\vec{E}_i$ perpendicular to the plane of the 2DES. The spin-orbit term in the Hamiltonian, called the *Rashba Hamiltonian*, is

$$H_{SO} = \alpha(\vec{s} \times \vec{k}) \cdot \hat{z}, \qquad (1)$$

where $\vec{s}$ is the carrier spin and the interaction between the field and carrier spin is described by α, the spin-orbit parameter. This term causes a spin splitting in the energy states $E(k, s)$ of the carrier. There are two populations (two spin subbands) of electrons, $n_\uparrow$ and $n_\downarrow$, with spin-split energies given by [Fig. 1(b)]

$$E(k, s) = E_0 + \frac{(\hbar k_x)^2}{2m^*} \pm \frac{1}{2}\alpha k_x. \qquad (2)$$
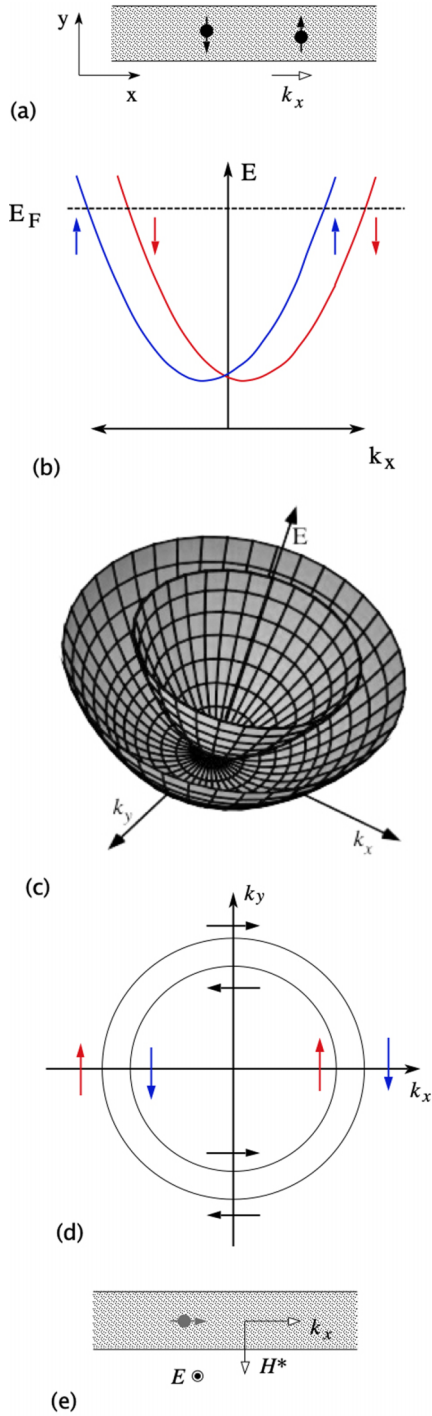
(a)

(b)

(c)

(d)

(e)

FIG. 1. (a) Schematic top view of a narrow wire mesa lithographically patterned from high-mobility 2DES with a Rashba SOI. Spin-up and spin-down carriers have momentum along the $\hat{x}$ axis. (b) Spin-orbit splitting of the energy dispersion of the carriers. (c) The Fermi sea is the conjoined paraboloid that results from revolving the dispersion curves about the vertical axis. (d) The Fermi surface is comprised of two concentric circles, obtained as a slice of the Fermi sea by a plane taken at the Fermi energy. Spin eigenstates are shown for momentum states along the $\hat{x}$ and $\hat{y}$ axes. (e) Spin-polarized carriers injected with spin orientation along $\hat{x}$ have a superposition of $\pm k_y$ momentum states. The intrinsic electric field is along the $\hat{z}$ axis. There is an effective magnetic field, $-H^*\hat{y}$, in the rest frame of the weakly relativistic carriers.

Parameter α is material specific and also is a function of any applied gate voltage, $\alpha = \alpha(V_G)$, m^* is the electron mass, $\hbar$ is Planck's constant divided by 2π, and E_0 is the energy at the bottom of the band. In the Datta-Das model, α uniquely depends on details of the heterostructure and the quantum well.

For the system described by Eq. (2), the Fermi sea is described by two conjoined paraboloids [Fig. 1(c)], given by revolving the two subbands in Fig. 1(b) about the E axis [13]. The Fermi surface is the slice of the Fermi sea that intersects the plane at the Fermi energy. As shown in Fig. 1(d), the Fermi surface is two concentric circles in the k_x-k_y plane. The outer (inner) circle has clockwise (counterclockwise) spin orientation.

The Datta and Das prediction of a ballistic spin precession effect is derived using the spin-orbit parameter α, but some physical insight about the precession can be gained by noting that the carrier Fermi velocity is weakly relativistic. As depicted in Fig. 1(e), an electric field E_z will transform as an effective magnetic field H_y^* in the frame of the carrier having momentum k_x. An electron injected along the k_x axis with spin orientation along the same axis will precess about the $\hat{y}$ axis because of the torque $\vec{s} \times \vec{H}^*$, and the spin-orbit term αk_x can be associated with the effective Zeeman energy $\mu_B H^*$. This model will be presented in greater detail below.

The Datta-Das calculation can be summarized by considering the electron in Fig. 1(e). As seen in Fig. 1(d), the spin eigenstates are parallel with the k_y axis, and the wave function of the injected carrier must be a superposition of states $\langle k_{x1}, s_{y,\downarrow} \rangle$ and $\langle k_{x2}, s_{y,\uparrow} \rangle$:

$$E(k_{x1}, s_{y,\downarrow}) = E_0 + \frac{(\hbar k_{x1})^2}{2m^*} - \frac{1}{2}\alpha k_{x1},$$

$$E(k_{x2}, s_{y,\uparrow}) = E_0 + \frac{(\hbar k_{x2})^2}{2m^*} + \frac{1}{2}\alpha k_{x2}.$$

Requiring the energies to be equal, we can find the difference $k_{x1} - k_{x2}$:

$$\frac{\hbar^2}{2m^*}\left(k_{x1}^2 - k_{x2}^2\right) = \alpha(k_{x1} + k_{x2}).$$

For a spin injected with initial orientation along $\hat{x}$, traveling with a ballistic trajectory, the precessional angle θ accumulated when it traverses a distance L is [10]

$$\Delta\theta = (k_{x1} - k_{x2})L = \frac{2m^*\alpha L}{\hbar^2}. \qquad (3)$$

Note that $\Delta\theta$ is independent of k_x. This is important experimentally because observing the Datta-Das precession does not require a one-dimensional wire. There is evidence that the magnitude of the effect may be larger in a channel with narrow width, but it is not necessary to have transport with a single k_x value.

Given an integrated method for injecting a spin-polarized electron at one position and detecting the phase angle $\Delta\theta$ of the spin orientation at a position at distance L, Eq. (3) then shows explicitly the two methods for a demonstration of the precessional oscillation that were introduced above: (I) With L fixed, a gate voltage can be varied to modulate

$\alpha(V_G)$ and variations of $\Delta\theta$ can be recorded. (II) With α fixed, measurements of $\Delta\theta$ can be made on a set of samples that are identically prepared except for varying length L. Results of both techniques will be reviewed in this paper.

A. Spin injection technique and a nonstandard geometry

The method for injecting spin-polarized electrons and detecting the spin polarization and phase angle of those electrons at a second electrode comes from the *spin injection* technique [14]. The technique is common knowledge within the magnetism and spintronics subfields, and in the following a brief review is given for readers outside of these topical areas.

Building on early theoretical and experimental work on carrier transport in ferromagnetic materials, from Mott [15] and Meservey [16], the spin injection/detection technique [17] was developed for diffusive transport. It demonstrated that a portion of a steady state electric current driven from a single domain ferromagnetic electrode (F1) into a nonmagnetic material would be spin polarized and a nonequilibrium population of polarized electrons, called a spin accumulation $\tilde{M}$, would diffuse into the nonmagnetic (N) material for a distance of a spin diffusion length, $\delta_s = \sqrt{D\tau_s}$, with D the carrier diffusion constant and τ_s the spin relaxation time in N. This length is the same as that which is measured in the analogous phenomenon of transmission electron spin resonance (TESR), with the substitution $\tau_s \approx T_2$, where T_2 is the transverse spin relaxation time. A second ferromagnetic electrode (F2) could be fabricated with interfacial contact to N, at a distance comparable with δ_s. When F2 is connected with a high-impedance voltmeter, a converse effect of spin injection develops a small voltage at F2. The voltage is proportional to the density of polarized carriers in the vicinity of the N-F2 interface and F2 is an effective spin detector.

In practice, F1 and F2 are microfabricated ferromagnetic films, typically using transition ferromagnetic materials such as $Ni_{0.8}Fe_{0.2}$ (Permalloy). The polarization efficiency, for both injection and detection, of such a film is the order of a few percent and spin detection voltages are typically small. In order to minimize background ohmic voltages, an unconventional geometry was developed for the first spin injection demonstration [14] and has been used in subsequent experiments [18,19]. Often called the "nonlocal geometry," Fig. 2(a) shows a schematic top view of a narrow "wire" of sample material N that extends along the x axis. For this initial discussion, we ignore the gate and dielectric, as well as length ℓ. Narrow electrode F1 spans the width of the wire near its center, $x = 0$. When bias current I is injected at F1 and grounded at the left end of the wire, $x = -b$, there is a linear voltage drop from $x = 0$ to $-b$, depicted by the regularly spaced equipotential (dotted-dashed) lines in Fig. 2(a). However, there is no net current flow in the region $x > 0$ and the wire is at a constant potential from $x = 0$ to $x = b$. A voltage measurement between the end of the wire $x = b$ and a narrow electrode that spans the wire at $x = L$ is necessarily a null measurement, $V = 0$.

Injected spin-polarized electrons diffuse equally along $\pm\hat{x}$. The density of diffusing spin-polarized electrons is depicted in Fig. 2(a) by the shaded region, with darker shades representing higher density. For a ferromagnetic electrode F2,
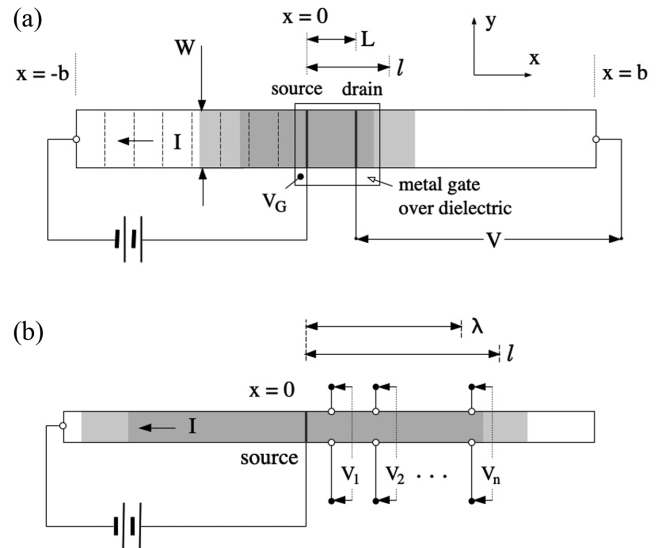

FIG. 2. (a) Nonlocal geometry that is typical of spin injection/detection experiments. The shaded gray areas represent the density of diffusing carriers, decreasing exponentially on either side of $x = 0$, for standard spin diffusion experiments in metals. The gray areas represent the density of ballistic carriers for spin injection experiments in the Datta-Das structure. The gate electrode is an addition for the Datta-Das structure. (b) The nonlocal geometry applied to a Datta-Das oscillation measurement using method II, explained in the text. Spin phase detection uses the spin Hall effect and a number of Hall crosses with varying distance L from the injector.

a measurement V records a spin-dependent voltage that is relatively high (low) when the magnetization orientation $M2$ is parallel (antiparallel) with $M1$. Since $V = 0$ in the absence of nonequilibrium spin effects, a measurement in this geometry uniquely discriminates against any background voltages. Both films F1 and F2 are sufficiently thin that magnetizations $M1$ and $M2$ are constrained to lie in the x-y plane and constructed to have a magnetization anisotropy so that $M1$ and $M2$ can be determined and retained using small external fields.

Structures of the kind in Fig. 2(a) are sometimes called "lateral spin valves" or "nonlocal lateral spin valve" (NLSV) to distinguish them from the thin-film magnetic sandwich structures which are simply called "spin valves." The structure in Fig. 2(b) is a variation of the nonlocal geometry used for method II and will be discussed further below. Regarding the lateral spin valve in Fig. 2(a), the spin diffusion length in N can be determined by measuring the spin accumulation at several electrodes with variable distance x from the injector. Alternatively, the spin relaxation time can be determined by the Hanle effect [20], applying an external magnetic field along an axis perpendicular to the $\hat{z}$, $H_\perp$. In a direct analog of TESR, the steady state diffusion of $\tilde{M}$ in the presence of $H_\perp$ results in a Lorentzian line shape of $\tilde{M}(H_\perp)$ at a single detecting electrode. Relaxation time τ_s is deduced from the Lorentzian. For ballistic electrons, application of field $H_\perp$ would result in a measured voltage V that varied periodically with L. Known as Larmor waves, this effect is observed with TESR [21], and it is a direct analog with the Datta-Das effect.

B. Spin injection in semiconductors: Practical considerations

Applying the spin injection technique to semiconducting materials involves two issues worthy of discussion. First, the details of charge and spin transport at an interface between two metals are fairly straightforward. By contrast, it is possible that spin transport may be less robust for the case of a metal-semiconductor interface. This question caused considerable confusion [22] and was finally clarified by Rashba [23]. The issue of conductance mismatch at the interface was first treated by Johnson and Silsbee [24] for any nonmagnetic material. The relevant parameters are the resistivities of the ferromagnetic and the nonmagnetic (metal of semiconductor) materials, ρ_f and ρ_n, respectively, the resistance of the interface R_i, and spin diffusion lengths in both N and F, $\delta_{s,n}$ and $\delta_{s,f}$. Specifically, the efficacy of spin transport across the interface is governed by the relative values of three resistances (units of resistance per unit area): the intrinsic interface resistance R_i, the resistance of a length of nonmagnetic material equal to a spin diffusion length, $r_n = \rho_n \delta_{s,n}$, and the resistance of a length of ferromagnetic material equal to a spin depth, $r_f = \rho_f \delta_{s,f}$. It also is governed by the fractional polarization of carriers near the Fermi surface in F and the fraction of polarized carriers that the interface can deliver to N, p_f and η, respectively. The general solution for the fraction of electric current J_e that is delivered across the interface as spin-polarized current J_M is [24]

$$J_M = \frac{\eta \mu_B}{e} J_e \left[\frac{1 + G(p_f/\eta)r_f(1-\eta^2)/(1-p_f^2)}{1 + G(1-\eta^2)[r_n + r_f/(1-p_f^2)]} \right], \quad (4)$$

where μ_B is the Bohr magneton and e the electron charge. For metal films, typical values of the resistances are estimated [25]: $r_f \sim 10^{-11} \ \Omega \ \text{cm}^2$, $r_n \sim 2 \times 10^{-11}$–$2 \times 10^{-10} \ \Omega \ \text{cm}^2$, and $R_i \approx 10^{-11} \ \Omega \ \text{cm}^2$. Since all of the characteristic values fall within a range of a factor of ten, all of the terms in Eq. (4) are important for metal films.

One limiting case of Eq. (4) is that of low interfacial resistance, $R_i \rightarrow 0$, and the equation reduces to the simpler form [26],

$$J_M = p_f \frac{\mu_B}{e} J_q \left[\frac{1}{1 + (r_n/r_f)(1-p_f^2)} \right]. \quad (5)$$

The polarization of the injected current is reduced by a backflow of nonequilibrium spins from N to F. The net polarization across the interface is independent of η and is reduced from that in the bulk ferromagnet by the resistance mismatch factor $(1 + M')^{-1} = [1 + (r_n/r_f)(1-p_f^2)]^{-1}$. Using estimates for r_f and r_n, and R_i for UHV-deposited F/N metal sandwich films, the mismatch factor can be as large as $M' \sim 20$.

The opposite limiting case is that of high interfacial resistance. Spin accumulation in N can be large but the resistive barrier prevents back diffusion. The nonequilibrium spin population in F remains small, and therefore the voltage drop across the interface is almost entirely due to R_i. The interfacial magnetization current is now given by [24]

$$J_M = \eta \frac{\mu_B}{e} J_q, \quad (6)$$

and the fractional polarization is dominated by the phenomenological interface parameter η. The resistive barrier
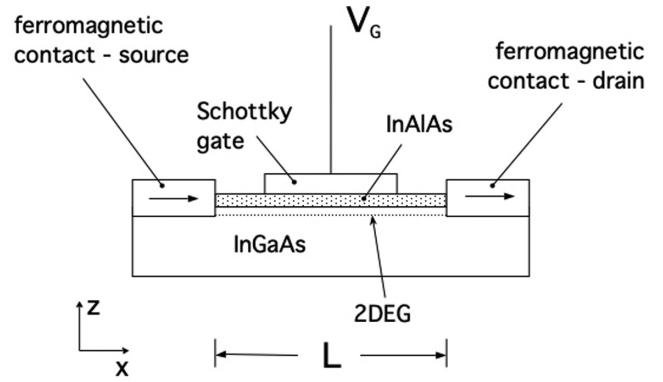

FIG. 3. Cross-sectional schematic of the spin injected FET (spin FET) proposed by Datta and Das [10].

may be asymmetric with respect to spin and, in general, the limit $\eta \leqslant p_f$ is imposed. For structures involving transport across a ferromagnetic metal film/semiconductor interface, the presence of a Schottky barrier introduces a large resistance R_i and Eq. (6) is valid. The experiments described herein use high-mobility indium arsenide heterostructures, which are known to have low Schottky barriers. As described below, thin tunnel barriers were formed between the InAs 2DES and the ferromagnetic metal electrodes and provided a high interface resistance. While this topic was a source of confusion, Rashba clarified this confusion [23] with a careful and definitive tunneling calculation. Rashba's results confirmed the above model when parameters and limits are properly identified.

A second issue, briefly controversial at one time but of less concern, is the presence of magnetic fields that may be proximal to ferromagnetic films. Associated with ferromagnetic metal films are fringe magnetic fields that are part of the "demagnetizing field." The magnitude of these fields can be large near the edges of the film. These fringe fields have little effect on carrier transport in metals. However, the Hall coefficient in semiconductors is substantially large and the fields may affect transport in a semiconductor device. Measurements of the magnitudes of the fringe fields [27] and direct measurements of the Hall effect driven by these fields [28] found that typical values are the order of 10^{-2} T or less. These fields are negligible in the experiments reported below, where the transport is modulated by the effective Rashba field of order 1 T.

II. METHOD I: THE DATTA-DAS DEVICE

Datta and Das proposed a simple InGas field-effect structure (Fig. 3), often called a spin-injected FET or spin FET. In their structure, a ferromagnetic source and drain are connected by a two-dimensional electron gas (2DEG) channel. The magnetizations of both source and drain were oriented along the axis of the channel, x axis. An intrinsic electric field E_z perpendicular to the 2DEG plane transforms, as discussed above, in the rest frame of the weakly relativistic carriers, as an effective magnetic field H_y^*. Carriers are injected at the source with their spin axes oriented along $\hat{x}$, precess under the influence of H_y^*, and arrive at the drain with a spin phase ϕ that depends on their time of transit, $\phi \propto L/v_F$, where v_F is

the Fermi velocity. By applying a gate voltage to the channel, the field E_z, the effective field H_y^*, and spin phase ϕ could be varied and a modulation of source-drain conductance as a function of V_G would result.

The nonlocal geometry of Fig. 2(a) can be adapted to the Datta-Das device. In a different description of Fig. 2(a), the gradient of gray shadings represents the density of spin-polarized ballistic electrons. The ferromagnetic gate is fabricated at a distance L less than the ballistic mean free path ℓ. A dielectric layer and a thin-film metal gate are fabricated to cover the channel between source and drain, and a variable gate voltage V_G can be applied. An external magnetic field applied along the x axis, $H \sim 0.1$ T, aligns the magnetizations $M1$ and $M2$ aligned parallel and along $\hat{x}$. Method I experiments are performed by measuring the drain voltage $V(V_G)$ as V_G is varied.

An excellent materials system for demonstrating Datta-Das oscillations is a single quantum well (SQW) in an epitaxial indium arsenide heterostructure. This two-dimensional electron system (2DES) has carriers with a ballistic mean free path of 1 µm or more at 4 K, and there is a very large spin-orbit interaction. The SOI can cause spin precession of a ballistic electron with a spatial wavelength $\lambda \ll \ell$. Using high-resolution electron beam lithography, a device structure can be fabricated to have a narrow channel with current and voltage electrodes with sufficiently small separation, $L < \ell$.

A. Detailed transport model

A pedagogical model [11] is useful for a detailed understanding of the experiment and is described with reference to Fig. 4. As mentioned above, the Rashba SOC mechanism in this 2DES derives from the structural asymmetry of the confining potential of the SQW. A doping layer inserted on one side of the SQW, or band bending that results from boundary conditions imposed by a surface, are examples of a structural asymmetry. The gradient of the confining potential represents an intrinsic electric field; fields on opposite sides of the SQW have opposite sign but do not cancel because of the structural asymmetry. It follows that there is a residual intrinsic electric field at the position of the 2DES. The field is perpendicular to the plane of the substrate (and of the 2DES) and has substantial magnitude even in the absence of gate voltage.

In Figs. 4(a) and 4(b), a current source is connected to a ferromagnetic film injector that has in-plane magnetization with orientation along the x axis of a narrow 2DES channel. Using the nonlocal geometry, the current is grounded at the left end of the channel. A ferromagnetic electrode detector is added to the structure, distance L from the injector, with its magnetization also along the x axis. Spin-polarized carriers are injected into the channel with the spin axis aligned along the x axis. A fraction of the injected carriers have ballistic trajectories along the $+\hat{x}$, moving with a weakly relativistic Fermi velocity, $v_{F,x} \sim c/300$, where c is the speed of light. If the intrinsic electric field is negligible and no gate voltage is applied ($V_G = 0$), then $H^* = 0$ and the carrier spin has the same orientation for the lifetime of the trajectory [Fig. 4(a)]. The detected voltage V is relatively high [Fig. 4(c)].
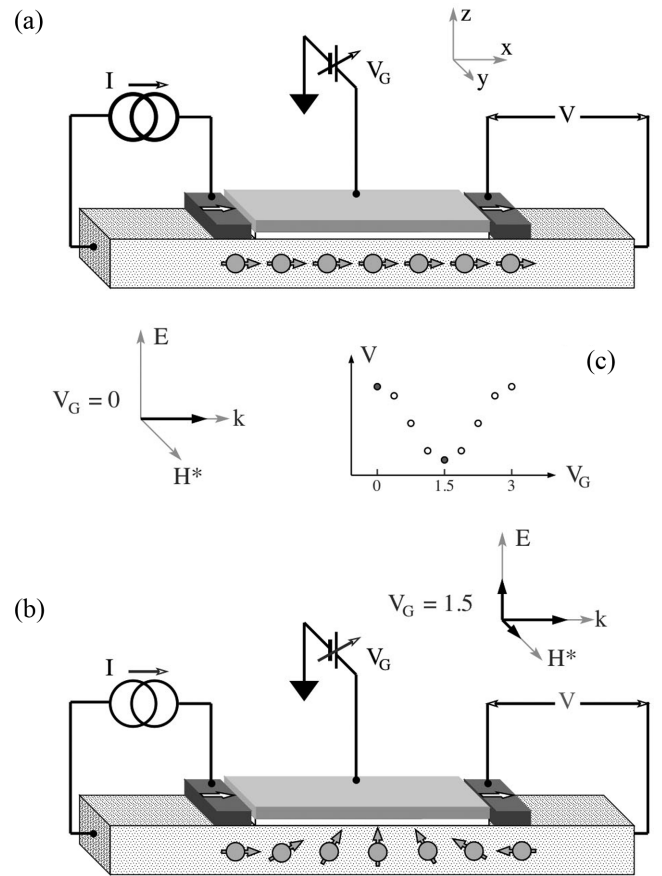

FIG. 4. Schematic representation of the Datta-Das experiment, adapted to the nonlocal lateral spin valve (NLSV) geometry as method I. In the pedagogical model described in the text, the intrinsic electric field is negligible but the gate voltage V_G can strongly modulate the field $\vec{E}$. (a) $V_G = 0$. The electric field is negligible. The detector magnetization orientation and the spin orientation of proximal carriers are parallel, and detector voltage V is high [solid symbol in (c)]. (b) $V_G = 1.5$ V (chosen to correspond with spin precession by π rad). The detector magnetization orientation and the spin orientation of proximal carriers are antiparallel, and detector voltage V is low [solid symbol in (c)]. (c) As V_G is varied, the wavelength λ changes and the detector records a periodic conductance oscillation $\Delta V(V_G)$. This figure is reproduced from Ref. [11].

When $E_z \neq 0$, the field, in the rest frame of the carrier, is transformed as an effective magnetic field H^*. In this case, electrons precess under the torque of the effective field. Figure 4(b) depicts the case with the value of V_G chosen such that H^* causes spin precession by π rad during the transit from injector to detector. The carrier spin is antiparallel with the detector magnetization at position $x = L$, and the detected voltage V is relatively low [Fig. 4(c)]. By monotonically increasing V_G, the magnitude of H^*, the spin-orbit parameter α, and the wavelength $\lambda(\alpha)$ all change and the detector voltage at fixed L varies between the peak and trough values. This was the prediction of Datta and Das [10].

As mentioned earlier, Datta-Das oscillations are an analog of Larmor waves. The controlling experimental parameter is an electric field for the former and a magnetic field for the latter. Larmor waves are observed in transmission electron

spin resonance (TESR) experiments [21]. A thin, high-purity nonmagnetic metal foil is mounted between send and received microwave cavities. At low temperature, the ballistic mean free path of conduction electrons in N may be longer than the thickness of the coil. If this is the case, the detected microwave power will show sinusoidal waves, with a wavelength that corresponds to the Larmor frequency of the ballistic carriers, superposed on the resonant Lorentzian feature that results from diffusive transport. For the Datta-Das oscillations, the SOI in the 2DES of a spin FET is very large and the spin relaxation rate $1/\tau_s$ is very rapid. There is no steady state spin accumulation because injected spin orientation becomes random after only a few scattering events. The Hanle effect, which is the diffusive analog of the TESR Lorentzian, is not observed, even though the Datta-Das ballistic-electron oscillations are present.

B. Method I results

A demonstration of the Datta-Das conductance oscillations using a variable gate voltage was provided by Koo *et al.* [11]. The devices consist of two $Ni_{81}Fe_{19}$ electrodes on top of an InAs high electron mobility transistor (HEMT) channel and a gate electrode. The InAs HEMT was grown by molecular beam epitaxy on a semi-insulating InP (100) substrate. The single quantum well, which functions as a 2DES channel, has a depth of 35.5 nm from the top surface. Bilayers of InAlAs/InGaAs form both the top and bottom barrier layers. Doping is provided by an $n+$ layer of InGaAs below the SQW. The carrier density and mobility of the 2DES are $n_S = 1.8 \times 10^{12}$ to 2.8×10^{12} cm^{-2} and $\mu = 50\,000$–$60\,000$ cm^2 V^{-1} s^{-1} at temperature $T = 1.8$ K, respectively. The channel, defined by a mesa etch, is oriented with x along the $\langle 110 \rangle$ direction and has a width $w = 8$ μm. The two ferromagnetic (FM) electrodes were fabricated with electron beam lithography, thin-film deposition, and lift-off and have lateral dimensions of 0.4×80 and 0.5×40 μm. A thin aluminum oxide layer was deposited prior to deposition of the ferromagnetic layer, providing an appropriate interface transport barrier R_i. Samples were made with FM electrode spacings of $L = 1.25$ and 1.65 μm, measured center to center. After fabrication of the structure, the device was covered by a dielectric and a metal gate electrode.

Figure 5 shows examples of the observed Datta-Das conductance oscillation. A magnetic field, with magnitude $B_{a,x} = 0.5$ T, is externally applied to orient the source and drain magnetizations to be along the $\hat{x}$ axis. The gate voltage is varied monotonically over the range $-3 \leqslant V_G \leqslant 3$ V while the nonlocal channel conductance is measured. Describing the top (gray) trace ($L = 1.65$ μm) first, the injected spin orientation along $+\hat{x}$ is perpendicular to the effective magnetic field. As described above, an oscillation of the voltage detected at the drain, as a function of gate voltage V_G, is observed because the rate of spin precession is proportional with gate voltage. The range of V_G is sufficiently large that Fig. 5 shows more than a full cycle of conductance oscillation. Data for a similar spin FET, with $L = 1.25$ μm, also are shown in Fig. 5 as the bottom trace (black).

The fits shown in Fig. 5, for the voltage $V(V_G)$ recorded at the detector, were generated using the theory of Datta and
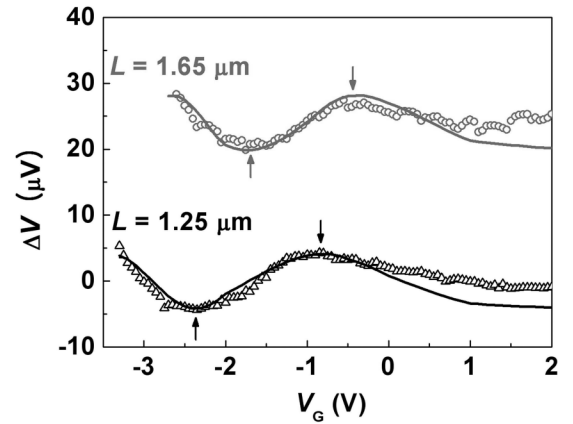

FIG. 5. Method I results. Datta-Das voltage oscillation $V(V_G)$ for two devices with different values of L. Symbols: Data. Solid lines: Fits. Details of the fits are found in Refs. [11,32]. This figure is reproduced from Ref. [11].

Das, Eq. (3),

$$V = A\cos(2m^*\alpha L/\hbar^2 + \phi). \quad (7)$$

In the above equation, ϕ is a small phase shift that may be related to shielding effects from the ferromagnetic films. The analysis required direct measurements of the oscillation amplitude A and the spin-orbit parameter $\alpha(V_G)$ for the range of gate voltages applied. The amplitude was determined using standard nonlocal lateral spin valve magnetoresistance measurements and a small in-plane magnetic field externally applied along the y axis. Hysteretic dips were observed in the small range of field between the values of switching field for the injecting and detecting films, where magnetizations $M1$ and $M2$ are antiparallel. The magnitude of the dips, $A = \Delta V = 6 \pm 0.2$ μV ($\Delta R = 6 \pm 0.2$ mΩ), is used as the amplitude of the fitting functions in Fig. 5. To determine the SOC parameter $\alpha(V_G)$, Shubnikov–de Haas oscillations were measured and the observed beat patterns were analyzed [11]. As examples of several parameters of interest, the spin-orbit parameter with zero gate voltage is $\alpha(0\ V) = 9.0 \times 10^{-12}$ eV m and the magnitude of the effective magnetic field (also at zero gate voltage) is $H_y^* = 8.5$ T.

The two data sets, for $L = 1.65$ and 1.25 μm, can be discussed by comparing their half wavelengths. As the channel length L decreases from 1.65 to 1.25 μm the half wavelength increases from $\Delta V_G = 1.24$ to 1.53 V. The detailed shape of the fit has been reproduced by numerical simulations [10] that are accompanied by a more detailed physical explanation.

III. METHOD II: CONSTANT α AND VARIABLE L

For method II, α is held fixed and the SOI is only provided by the intrinsic asymmetry of the single quantum well. There is no gate and no gate voltage is applied.

A. Experimental geometry

Measurements of $\Delta\theta$ can be made on a set of samples that are identically prepared except for varying length L. As with method I, the measurements are facilitated by using a nonlocal

geometry. Referring to Fig. 2(b), the bias current is supplied to a ferromagnetic electrode at $x = 0$ and grounded at the far left of the narrow "wire." Ballistic, spin-polarized electrons are injected in equal numbers to the right and left, along $\pm \hat{x}$. There is no net diffusive current to the right, and the region $x > 0$ is equipotential.

An experimental demonstration was provided by Choi *et al.* [12]. Instead of using a ferromagnetic film as a detector, the authors employed the spin Hall effect (SHE) [29,30]. They confirmed their measurements using the inverse spin Hall effect (ISHE) [31]. The detector took the form of a Hall cross with narrow transverse arms [Fig. 2(b)]. The spin Hall effect force $\vec{F}$ is a cross product of $\vec{v}_F$ and $\vec{s}$ and is perpendicular to both. Along the ballistic-electron trajectory, $\vec{F}$ is maximum when $\vec{s}$ is along the z axis and here ΔV_H has maximum value, either positive or negative. When $\vec{s}$ is along the x axis, $\vec{F}$ is zero and $\Delta V_H = 0$. For a constant value of spin injected current, the voltage between the arms was measured as an external magnetic field H_x changed the magnetization orientation of the ferromagnetic injector from parallel to antiparallel with the x axis. Since this change corresponds to changing the initial spin orientation by π rad, the spin Hall voltage at the detector changes signs. The difference $\Delta V_H(x)$ is therefore proportional to the spin orientation $\vec{s}$ of the ballistic electrons at the detector position, x.

In Fig. 2(b), a linear array of electrodes extends over a region that is longer than the Datta-Das wavelength λ. The width of each voltage probe w_V must be much smaller than the wavelength, $w_v \ll \lambda$, and, in practice, limitations of lithographic fabrication require that a number n of individual samples must be made, one for each distance $x = L_n$. Any small fabrication error in the spatial offset of each pair of electrodes would result in a large offset resistance and voltage in the presence of diffusive current. The nonlocal geometry reduces such offsets substantially.

B. Method II results

A demonstration of the Datta-Das conductance oscillations using variable length L was provided by Choi *et al.* [12]. In these experiments, the width of the 2DES channel was 750 nm. The following sample characteristics were determined (at 1.8 K): carrier density $n = 2.0 \times 10^{12}$ cm^2, mobility $\mu = 60\,000$ cm^2 V^{-1} s^{-1}, and mean free path $\ell = 1.61$ μm. From the beat frequency in Shubnikov–de Haas measurements [11], the spin-orbit parameter was found to be $\alpha = 8.93 \times 10^{-12}$ eV m, at $V_G = 0$. Using these numbers and $m^* = 0.05 m_0$ ($m_0 = 9.1 \times 10^{-31}$ kg), the Datta-Das wavelength can be calculated, $\lambda = 0.54$ μm ($\ll \ell = 1.6$ μm).

Figure 6 plots values of $\Delta R_H(L)$ and two complete wavelengths of the conductance oscillation are observed. The fit represented by the dotted line in the figure uses the wavelength λ of Eq. (3), $\lambda = \pi \hbar^2 / \alpha m^*$,

$$\frac{\Delta V_H}{I} = \Delta R_H = A \cos(2\pi L / \lambda - \pi/2), \qquad (8)$$

where A is the measured amplitude. The solid line modifies the above expression by including an exponential decay $e^{-L/\ell}$, where the ballistic mean free path was independently determined [11], $\ell = 1.61$ μm. The only free fitting parameter is
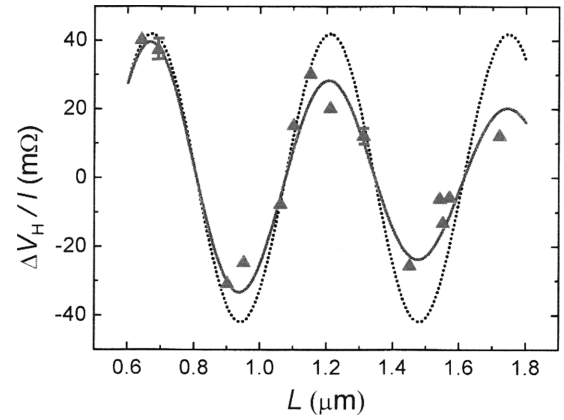

FIG. 6. Method II results. Resistance oscillation $\Delta V_H(L)/I$, where I is the bias current and the channel length is L. There are 14 individual sample devices, nominally identical. Each device has channel width $w_C = 0.75$ μm. $I = 0.1$ mA, $T = 1.8$ K. The dotted line fit is from the ballistic transport model, Eq. (3). The solid line fit is the same model modified to include the exponential decay of ballistic trajectories. Error bars are smaller than the symbols except where shown. This figure is reproduced from Ref. [12].

the amplitude, experimentally measured as ΔR_H for the sample device with $L = 0.64$ μm. It is important to note that there is no arbitrary phase shift in the data of Fig. 6; the data values are determined only by the injector and detector distance L. The authors provided further confirmation by adding a gate to one of the samples and making a method I measurement.

IV. SUMMARY

Four decades ago, Rashba's seminal theory of spin-orbit interactions in a high-mobility 2DES with an asymmetric confining potential opened the door to predictions of novel transport effects. Two decades later, Datta and Das proposed an experiment involving spin injection, detection, and spin precession of ballistic electrons caused by a gate voltage and the Rashba spin-orbit interaction. The nonlocal lateral spin valve geometry in two configurations was used to provide independent demonstrations of the Datta-Das conductance oscillations. An InAs single quantum well proved to be an ideal material. The carrier mean free path is longer than 1 μm at low temperature, and a large spin-orbit interaction modulates a Rashba field by several tesla with a gate voltage range of a few volts. High-precision electron beam lithography was used to fabricate mesa structures with narrow channels. In one configuration, the source and drain were thin-film ferromagnetic metal electrodes and the entire device was gated. The voltage at the drain, $V(V_G)$, showed oscillations as the gate voltage was varied. In a second configuration, 14 samples were prepared, each with a ferromagnetic thin-film source. The detected voltage for each sample was a function of the spin Hall effect and was measured with a Hall cross at a short distance from the source. The set of voltages from all samples, $V(x)$, showed the predicted oscillation. In both configurations, the results agreed very well with theory and confirmed the theories of Rashba and Datta and Das.

[1] R. J. Elliott, Theory of the Effect of Spin-Orbit Coupling on Magnetic Resonance in Some Semiconductors, Phys. Rev. **96**, 280 (1954).

[2] G. Dresselhaus, Spin-Orbit Coupling Effects in Zinc Blende Structures, Phys. Rev. **100**, 580 (1955).

[3] E. I. Rashba and V. I. Sheka, Symmetry of Energy Bands in Crystals of Wurtzite Type II. Symmetry of Bands with Spin-Orbit Interaction Included, Fiz. Tverd. Tela: Collected Papers **2**, 6276 (1959).

[4] G. Bihlmayer, O. Rader, and R. Winkler, Focus on the Rashba effect, New J. Phys. **17**, 050202 (2015).

[5] E. I. Rashba, Properties of semiconductors with an extremum loop. 1. Cyclotron and combinational resonance in a magnetic field perpendicular to the plane of the loop, Sov. Phys. Solid State **2**, 1109 (1960).

[6] W. Zawadzki and P. Pfeffer, Spin splitting of subband energies due to inversion asymmetry in semiconductor heterostructures, Semicond. Sci. Technol. **19**, R1 (2004).

[7] D. Stein, K. v. Klitzing, and G. Weimann, Electron Spin Resonance on GaAs - $Al_x Ga_{1-x}$As Heterostructures, Phys. Rev. Lett. **51**, 130 (1983).

[8] Yu. A. Bychkov and E. I. Rashba, Properties of a 2D electron gas with a lifted spectrum degeneracy, Sov. Phys. JETP Lett. **39**, 78 (1984).

[9] A. Manchon, H. Koo, J. Nitta, S. M. Frolov, and R. A. Duine, New perspectives for Rashba spin-orbit coupling, Nat. Mater. **14**, 871 (2015).

[10] S. Datta and B. Das, Electronic analog of the electro-optic modulator, Appl. Phys. Lett. **56**, 665 (1990).

[11] H. C. Koo, J. H. Kwon, J. Eom, J. Chang, S. H. Han, and M. Johnson, Control of spin precession in a spin-injected field effect transistor, Science **325**, 1515 (2009).

[12] W. Y. Choi, H. J. Kim, J. Chang, S. H. Han, H. C. Koo, and M. Johnson, Electrical detection of coherent spin precession using the ballistic intrinsic spin Hall effect, Nat. Nanotechnol. **10**, 666 (2015).

[13] R. H. Silsbee, Theory of the detection of current-induced spin polarization in a two-dimensional electron gas, Phys. Rev. B **63**, 155305 (2001).

[14] M. Johnson and R. H. Silsbee, Interfacial charge-spin coupling: Injection and detection of spin magnetization in metals, Phys. Rev. Lett. **55**, 1790 (1985).

[15] N. F. Mott, The electrical conductivity of transition metals, Proc. R. Soc. London, Ser. A **153**, 699 (1936).

[16] R. Meservey and P. M. Tedrow, Magnetic Field Splitting of the Quasi-particle States in Superconducting Aluminum Films, Phys. Rev. Lett. **25**, 1270 (1970).

[17] M. Johnson and R. H. Silsbee, Spin-injection experiment, Phys. Rev. B **37**, 5326 (1988).

[18] S. O. Valenzuela and M. Tinkham, Spin-polarized tunneling in room-temperature mesoscopic spin valves, Appl. Phys. Lett. **85**, 5914 (2004).

[19] X. Lou, C. Adelmann, S. A. Crooker, E. S. Garlid, J. Zhang, S. M. Reddy, S. D. Flexner, C. J. Palmstrom, and P. A. Crowell, Electrical detection of spin transport in lateral ferromagnet-semiconductor devices, Nat. Phys. **3**, 197 (2007).

[20] W. Hanle, ber magnetische Beeinflussung der Polarisation der Resonanzfluoreszenz, Z. Phys. **30**, 93 (1924).

[21] R. H. Silsbee, A. Janossy, and P. Monod, Coupling between ferromagnetic and conduction-spin-resonance modes at a ferromagnetic-normalmetal interface, Phys. Rev. B **19**, 4382 (1979).

[22] G. Schmidt, D. Ferrand, L. W. Molenkamp, A. T. Filip, and B. J. van Wees, Fundamental obstacle for electrical spin injection from a ferromagnetic metal into a diffusive semiconductor, Phys. Rev. B **62**, R4790 (2000).

[23] E. I. Rashba, Theory of electrical spin injection: Tunnel contacts as a solution of the conductivity mismatch problem, Phys. Rev. B **62**, R16267 (2000).

[24] M. Johnson and R. H. Silsbee, Thermodynamic analysis of interfacial transport and of the thermomagnetoelectric system, Phys. Rev. B **35**, 4959 (1987).

[25] R. Godfrey and M. Johnson, Spin injection in mesoscopic silver wires: Experimental test of resistance mismatch, Phys. Rev. Lett. **96**, 136601 (2006).

[26] M. Johnson and R. H. Silsbee, Ferromagnet-nonferromagnet interface resistance, Phys. Rev. Lett. **60**, 377 (1988).

[27] T. Clinton and M. Johnson, Mesoscopic magnetoquenched superconducting valve, Appl. Phys. Lett. **70**, 1170 (1997).

[28] M. Johnson, B. Bennett, J. J. Yang, M. M. Miller, and B. V. Shannabrook, Hybrid Hall effect device, Appl. Phys. Lett. **71**, 974 (1997).

[29] M. I. Dyakonov and V. I. Perel, Current-induced spin orientation of electrons in semiconductors, JETP Lett. **13**, 467 (1971).

[30] J. Hirsch, Possibility of orienting electron spins with current, Phys. Rev. Lett. **83**, 1834 (1999).

[31] S. O. Valenzuela and M. Tinkham, Direct electronic measurement of the spin Hall effect, Nature (London) **442**, 176 (2006).

[32] A. N. M. Zainuddin, S. Hong, L. Siddiqui, S. Srinivasan, and S. Datta, Voltage-controlled spin precession, Phys. Rev. B **84**, 165306 (2011).